

# First Landau Level Physics in Second Moiré Band of 2.1° Twisted Bilayer MoTe<sub>2</sub>

Cheong-Eung Ahn,<sup>1,2,\*</sup> Wonjun Lee,<sup>1,2,\*</sup> Kunihiro Yananose,<sup>3</sup> Youngwook Kim,<sup>4</sup> and Gil Young Cho<sup>1,2,5,†</sup>

<sup>1</sup>*Department of Physics, Pohang University of Science and Technology, Pohang, 37673, Republic of Korea*

<sup>2</sup>*Center for Artificial Low Dimensional Electronic Systems,*

*Institute for Basic Science, Pohang 37673, Korea*

<sup>3</sup>*Korea Institute for Advanced Study, Seoul 02455, Korea*

<sup>4</sup>*Department of Physics and Chemistry, Daegu Gyeongbuk Institute of*

*Science and Technology (DGIST), Daegu 42988, Republic of Korea*

<sup>5</sup>*Asia-Pacific Center for Theoretical Physics, Pohang, Gyeongbuk, 37673, Korea*

(Dated: March 29, 2024)

The recent experimental discovery of the fractional quantum spin Hall effect in twisted bilayer MoTe<sub>2</sub> at a twist angle of 2.1 degrees highlights the unique properties of its second moiré band. Inspired by this finding, we conduct a comprehensive theoretical investigation of the half-filled second moiré band at this angle, utilizing an effective continuum model. Our analysis reveals that the band not only exhibits characteristics akin to the first Landau level,  $K = \int_{\text{BZ}} d^2\mathbf{k} \text{tr} \eta(\mathbf{k}) \approx 3$ , but also that its projected Coulomb interaction strikingly mirrors the Haldane pseudopotentials of the first Landau level. They together strongly indicate the potential emergence of a non-Abelian fractional quantum anomalous Hall state at the half-filling under the Coulomb interactions. By performing exact diagonalization calculations, we validate this hypothesis and construct a global phase diagram around this non-Abelian fractional quantum anomalous Hall states. We also introduce a novel metric of 1LL-ness of a band, which quantitatively measures the alignment of the projected Coulomb interaction with the Haldane pseudopotentials in Landau levels. This metric is then compared with the global phase diagram including the non-Abelian fractional quantum anomalous Hall state, revealing its utility in predicting the parameter region of the 1LL-ness. Finally, we discuss the potential implications on experiments.

Twisted moiré materials have unveiled various exciting quantum phenomena, encompassing Mott insulators [1, 2], strange metals [3], superconductivity [4, 5], and integer and fractional quantum anomalous Hall (FQAH) effect [6–11]. Even more surprisingly, recent transport experiments on twisted bilayer MoTe<sub>2</sub> (tMoTe<sub>2</sub>) around a twist angle  $\theta \sim 2.1^\circ$  have hinted at the emergence of integer quantum spin Hall effects at the even-integer hole fillings of the moiré bands, alongside a fractional quantum spin Hall (FQSH) effect at a hole filling  $\nu_h$  of 3 [11]. Intriguingly, the transport signature at  $\nu_h = 3$  is consistent with the emergence of a non-Abelian, half-filled FQAH state in one valley and its time-reversal conjugate in the opposite valley. On the other hand, the absence of Abelian FQAH states, which were previously reported in the first moiré band at  $\theta \sim 3.7^\circ$  [6–9], points to a distinct nature of the second moiré band at  $\theta \sim 2.1^\circ$ .

Inspired by these intriguing findings, we embark on an in-depth theoretical examination of the half-filled second moiré band at  $\theta \sim 2.1^\circ$ , with a specific focus on the characteristics of the projected Coulomb interaction. Our analysis is based on the continuum description of the density functional theory (DFT) band structure for tMoTe<sub>2</sub> at this angle [12]. According to [12], each of the three moiré bands ( $a = 1, 2, 3$ ) exhibit a valley-projected Chern number of  $C_{\uparrow,a} = +1$  with  $C_{\uparrow,a} = -C_{\downarrow,a}$ , indicating a balance between opposite spin orientations. This pattern aligns with the experimental observations of integer quantum spin Hall states at even-integer hole fillings [11], setting it apart from the sequence of Chern num-

bers identified in moiré bands around a twist angle of  $\theta \sim 3.7^\circ$ . The continuum model indeed well captures this distinction [Table I] and also the sequence of Chern numbers unique to tMoTe<sub>2</sub> at  $\theta \sim 2.1^\circ$  [13].

In this Letter, we use the continuum model Eq.(1) fitted with [12] and uncover the first Landau level (1LL) physics in the second moiré band of tMoTe<sub>2</sub> near  $\theta \sim 2.1^\circ$ . This contrasts with the first moiré band of the tMoTe<sub>2</sub> for  $\theta \gtrsim 3.9^\circ$ , which is widely recognized for its resemblance to the lowest Landau Level (LLL) [14–19]. Essentially, we observe that the projected Coulomb interaction closely mirrors the Haldane pseudo-potential in 1LL while the band fulfills the known 1LL trace condition  $K = \int_{\text{BZ}} d^2\mathbf{k} \text{tr} \eta(\mathbf{k}) \approx 3$  [20, 21]. These two criteria are in principle independent to each other, and should both be satisfied to best mimic the physics of 1LL. Motivated by this observation, we present a new metric Eq.(2) for 1LL-ness of the band, which quantifies the similarity of the projected Coulomb interaction to the Haldane pseudopotentials in 1LL. Within the Coulomb interaction, through exact diagonalization (ED) calculations, we also demonstrate the emergence of a non-Abelian FQAH at  $\nu_h = 2 + 1/2$  from the second moire band, whose ground state degeneracy agrees with the Pfaffian state at 1LL [21–23]. In addition, we compare the global phase diagram around this FQAH with the values of our new metric Eq.(2), which reveals its utility in predicting the parameter region of the 1LL-ness.

Let us compare our findings with the existing studies. First, [24] explored the first moiré band of tMoTe<sub>2</sub> at  $\theta \sim$

angle	$v_1$	$\psi$	$\gamma_1$	$v_2$	$\gamma_2$	Ref.
$\gg 1^\circ$	8	$-89.6^\circ$	-8.5	0	0	[25]
$4.4^\circ$	11.2	$-91^\circ$	-13.3	0	0	[19]
$3.9^\circ$	7.5	$-100^\circ$	-11.3	0	0	[19]
-	9.2	$-99^\circ$	-11.2	0	0	[26]
-	20.8	$-107.7^\circ$	-23.8	0	0	[27]
-	17.0	$-107.7^\circ$	-16.0	0	0	[28]
-	16.5	$-105.9^\circ$	-18.8	0	0	[18]
-	7.94	$-88.43^\circ$	-10.77	20.00	10.21	[18]
-	9.45	$-85.23^\circ$	-12.20	24.99	13.12	[12, 13]
$2.1^\circ$	20.51	$-61.49^\circ$	-7.01	-9.08	11.08	[12, 13]
$1.2^\circ$	24.93	$-36.61^\circ$	-5.06	-24.18	30.98	[12, 13]

TABLE I: **Continuum model parameters.** The parameters  $v_1$ ,  $\gamma_1$ ,  $v_2$ ,  $\gamma_2$  are given in units of meV.

$3.9^\circ$  with three-body interactions. On the other hand, [21] investigated a skyrmion Chern band model, which captures the essence of twisted bilayer transition metal dichalcogenides. Within this model, [21] also pointed out the 1LL-like nature of the second moire band and emergence of the non-Abelian FQAH, using the wavefunction overlap of the single-hole states in their model with corresponding 1LL states. Our work distinguishes itself by focusing directly on the second moiré band of a realistic continuum model at  $\theta \sim 2.1^\circ$  and revealing 1LL-ness of the second moire band via the projected Coulomb interactions.

**1. Continuum Model.** We start with the continuum model [25] of tMoTe<sub>2</sub> around the  $K$ -valley (with  $\hbar = 1$ )

$$\hat{h}_\uparrow = \begin{bmatrix} -\frac{(\hat{\mathbf{k}}-K_+)^2}{2m^*} + V_+(\hat{\mathbf{r}}) & \Gamma^*(\hat{\mathbf{r}}) \\ \Gamma(\hat{\mathbf{r}}) & -\frac{(\hat{\mathbf{k}}-K_-)^2}{2m^*} + V_-(\hat{\mathbf{r}}) \end{bmatrix}, \quad (1)$$

where  $m^*$  is the effective mass of the monolayer electron,  $K_\pm = R_{\pm\theta/2}K$  are the twisted  $K$  points of the top and bottom layers,  $V_\pm(\mathbf{r})$  and  $\Gamma(\mathbf{r})$  are the intralayer and interlayer moiré potentials, respectively. These potentials are considered up to valley-reduced inversion symmetric second harmonics [13, 18]. The Hamiltonian around the  $(-K)$ -valley is the time-reversal conjugate of Eq.(1). For tMoTe<sub>2</sub> at  $\theta \sim 2.1^\circ$ , we found the model parameters ( $v_1, \psi, \gamma_1, v_2, \gamma_2$ ) of Eq.(1) by fitting its band structure with the DFT result [12] along the high-symmetry lines in momentum space [13]. The resulting parameters are listed in Table I, whose band structure is in [Fig.1(a)].

A few comments are in order. First, we confirmed that the model parameters for  $\theta \sim 2.1^\circ$  produces the series of the Chern numbers, consistent with the DFT calculation [12] and also the experiment [11]. This supports the validity of our continuum model parameters beyond the numerical fitting. Secondly, from Table I, we observe a significant renormalization of the model parameters for  $\theta \sim 2.1^\circ$  relative to those for  $\theta \gtrsim 3.9^\circ$  [18, 19, 25–28]. As discussed in [12, 18], the higher harmonics in the model parameters are expected to play a significant role at smaller twist angles, and they can even

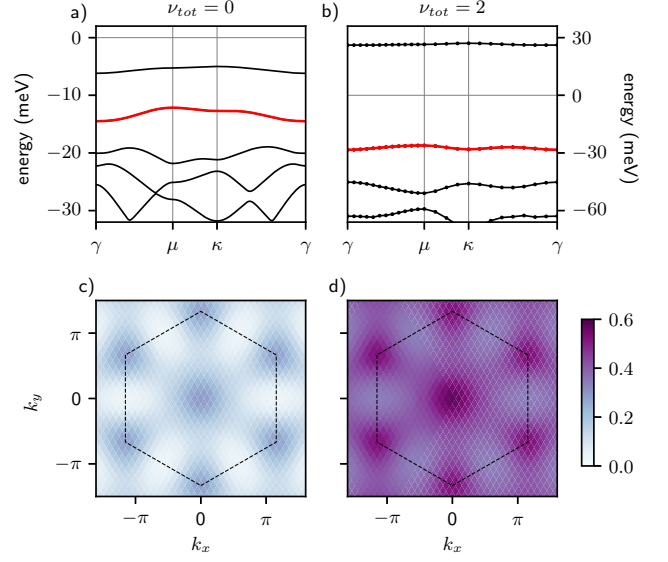


FIG. 1: (a) Band structure at  $\nu_h = 0$  and (b) its SCHF-corrected band structure at  $\nu_h = 2$  with  $\epsilon_r = 5.0$ . (c) Berry curvature and (d) trace of the Fubini-Study metric of the SCHF-corrected second moiré band. The black dashed line represents the moire BZ with  $a_M = 1$ .

undergo a rapid change in sign with twist angle. This is reflected in the sign of  $v_2$  for  $\theta \sim 2.1^\circ$  relative to those for  $\theta \gtrsim 3.9^\circ$ . Despite of these drastic differences in model parameters, the moire band widths at  $\theta \sim 2.1^\circ$  remain small, approximately 2.4 meV, signifying the importance of the interactions to fully comprehend the physics.

**2. Coulomb Interaction.** We assume the Coulomb interaction [15, 17, 19, 26, 27, 29, 30]

$$H = -\hat{h} + \frac{1}{2A} \sum_{\mathbf{p}} V_{\mathbf{p}}: \hat{\rho}_{\mathbf{p}} \hat{\rho}_{-\mathbf{p}}:$$

Here,  $\hat{\rho}_{\mathbf{p}} = \sum_{\tau, \mathbf{k}, \ell} \hat{c}_{\tau, \mathbf{k}+\mathbf{p}, \ell}^\dagger \hat{c}_{\tau, \mathbf{k}, \ell}$  is the density operator,  $A$  is the sample area, and the normal ordering is against  $\nu_h = 0$ , and

$$V_{\mathbf{p}} = \left( \frac{e^2}{4\pi\epsilon_0} \right) (2\pi\epsilon_r^{-1}) \frac{\tanh(p\xi/2)}{p},$$

where  $\xi$  is the gate distance and  $\epsilon_r$  is the relative permittivity. For simplicity, we set  $\xi = \infty$ , i.e., the unscreened Coulomb interaction, as its precise value has little effect on FQAHs due to the large size of the moire unitcell [17].

As the DFT band is obtained at  $\nu_h = 0$ , we use the self-consistent Hartree-Fock (SCHF) method to obtain the renormalized second moiré band at  $\nu_h = 2$ , its Berry curvature and trace of the Fubini-Study metric [Fig.1(b-d)]. We find that the Hartree-Fock correction makes the Berry curvature and trace of the Fubini-Study metric significantly more uniform [13], similar to the valley-polarized first moiré band at  $\nu_h = 1$  [15, 17, 19]. On the other hand,

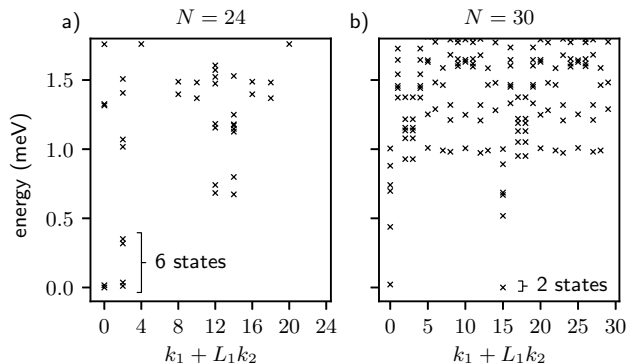


FIG. 2: Energy spectrum on a torus of (a)  $4 \times 6$ , and (b)  $5 \times 6$  unitcells.

the trace of the Fubini-Study metric, i.e.,  $\text{tr } \eta(\mathbf{k})$ , is much larger than the absolute Berry curvature, suggesting that the second moiré band is distinct from LLL-like bands [31–33]. Indeed, the quantum weight  $K = \int_{\text{BZ}} d^2\mathbf{k} \text{tr } \eta(\mathbf{k})$  for  $\epsilon_r = 5$  reaches 3.04 approximately, well satisfying a property of 1LL-like bands [20, 21], whereas the Chern number is  $C = 1$ . We note that while a mathematically precise criteria for 1LL-like bands has recently been proposed in [20], it requires the global information of band structures. Hence, a direct characterization of 1LL-like bands from local quantum geometry has yet to be found, as noted in [20].

**3. Non-Abelian FQAH.** Driven by the resemblance of the second moiré bands to 1LL, we undertake ED calculations to search for a non-Abelian FQAH state. Our analysis focuses on the half-filled, SCHF-corrected second moiré bands, within a system comprising  $4 \times 4$  unitcells. We first find that the ground state is fully valley-polarized for a wide range of twist angles  $\theta \in [1.5^\circ, 3.0^\circ]$  and dielectric constants  $\epsilon_r \in [2, 10]$ , under the assumption that all model parameters in Eq.(1) remain unchanged except  $\theta$ . This behavior mirrors that observed in the first moiré band within the Coulomb and dual-gate screened Coulomb interaction [17, 19, 27, 29, 34]. Building on this, below we narrow our ED investigation to a single valley, aiming to uncover the intricate characteristics of the ground state.

In [Fig.2(a,b)], we present the many-body energy spectra of a single valley for  $N = 4 \times 6$  and  $N = 5 \times 6$  unitcells at  $\epsilon_r = 5.0$  and  $\theta = 2.1^\circ$ . Importantly, we observe the emergence of six-fold and two-fold degenerate ground states for even and odd number of holes, matching precisely those of the Pfaffian state [22, 23], which strongly suggests the emergence of a non-Abelian FQAH.

**4. 1LL-like Projected Interactions.** While FQAHs require both the appropriate band structure and interactions, much of the previous literature [14–19, 21] focus largely on the band characteristics like the Fubini-Study metric to discuss the  $n$ LL-ness. Here, we focus on

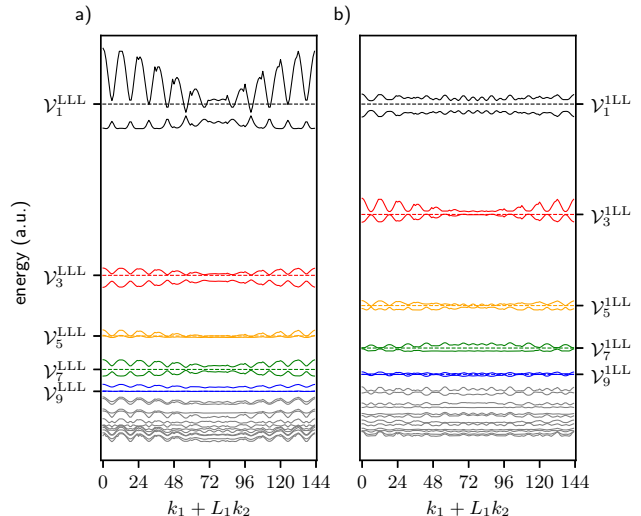


FIG. 3: Effective Haldane pseudopotentials of projected Coulomb interactions. The solid lines are the estimated Haldane pseudopotential of (a) the first moire band at  $\theta = 3.7^\circ$  and (b) the second moire band at  $\theta = 2.1^\circ$ . In both cases, we take  $\epsilon_r = 5$ . The dashed lines are the exact Haldane pseudopotentials of (a) LLL and (b) 1LL.

the nature of the projected Coulomb interaction in moire bands and compare them with those in LLs.

To have a fair comparison of the projected Coulomb interaction in the second moire band with that in 1LL, we calculate the effective Haldane pseudopotentials of the projected interaction from the energy spectrum of two holes [35]. When the band is completely flat and the projected interaction respects the translation symmetry, the energy levels of the two holes are expected to organize into pairs, irrespective of momentum. Then, the first highest pair’s energy is  $\mathcal{V}_1$ , the second pair’s energy is  $\mathcal{V}_3$ , the third pair’s is  $\mathcal{V}_5$ , and so forth. If the band under consideration perfectly mimics the physics of  $n$ LL, one expects that the pseudopotential will equal to those of the LL-level projected Coulomb interaction, namely the Haldane pseudopotentials  $\mathcal{V}_\ell^{n\text{LL}}$  ( $\ell = 1, 3, 5, \dots$ ), up to a global scale. For non-ideal bands, the pairs are split and show momentum dependence.

Spectacularly, we observe that the effective Haldane pseudopotentials of the projected Coulomb interaction in the SCHF-renormalized second moire band at  $\theta \sim 2.1^\circ$  [Fig.1(b)] is close to those of the 1LL-projected Coulomb interaction [Fig.3(b)]. This provides further support of the emergence of the 1LL-like non-Abelian FQAH in our ED calculation. Following the same calculation, we can also demonstrate that for the first moire band at  $\theta = 3.7^\circ$ , the effective pseudopotential of the projected Coulomb interaction is similar to the Haldane pseudopotential in LLL [Fig.3(a)], consistent with previous characterization of the first moire band in terms of quantum geometry [14–

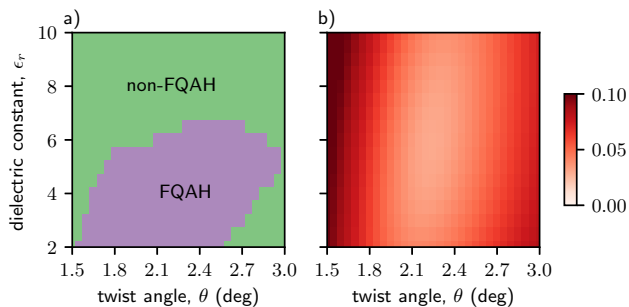


FIG. 4: (a) Phase diagram. (b) Value of 1LL-ness  $S$ , Eq.(2) for  $w_m = 1$  for  $m \leq 9$  and  $w_m = 0$  for  $m > 9$ .

19]. For the latter, we used the continuum model Eq.(1) with model parameters for  $\theta \sim 3.9^\circ$  [12, 13], also reported in Table.I. Finally, we observe that the projected Coulomb interaction in the third moiré band is also 2LL-like for  $\theta = 2.1^\circ$  and  $\epsilon_r = 5$ , along with the 2LL-like band characteristics  $K = \int_{\text{BZ}} d^2\mathbf{k} \text{tr} \eta(\mathbf{k}) \approx 5$  [13].

Motivated by this, we propose a quantitative metric for the  $n$ LL-ness of the projected interactions

$$S^2 = \frac{1}{N} \sum_{\mathbf{K}} \sum_{\ell=1}^{\infty} w_{2\ell+1} \left( \left| \frac{\tilde{E}_{\mathbf{K},2\ell-1} - E_0}{E_1 - E_0} - \frac{v_{2\ell-1}^{n\text{LL}}}{v_1^{n\text{LL}}} \right|^2 + \left| \frac{\tilde{E}_{\mathbf{K},2\ell} - E_0}{E_1 - E_0} - \frac{v_{2\ell}^{n\text{LL}}}{v_1^{n\text{LL}}} \right|^2 \right) \geq 0, \quad (2)$$

where  $\tilde{E}_{\mathbf{K},a}$  ( $a = 1, 2, 3, \dots$ ) are the energy levels of the total momentum sector  $\mathbf{K} = \mathbf{k}_1 + \mathbf{k}_2$  of the two holes in *descending* order, and  $E_1, E_0$  are the global scaling factors. Each  $\ell$ -th term in the sum is weighted by  $w_\ell \in [0, 1]$ . This metric measures both the deviation of the estimated pseudopotentials from those of  $n$ LL, and also the non-ideality of the band like the non-flatness and non-uniform quantum geometry. The smaller the metric  $S$  is, the band-projected interaction is closer to the 1LL-projected Coulomb interaction. Below, we will compare its value with the many-body phase diagram.

Let us remark a few important points on Eq.(2). First, the computation of  $S$  is much less costly than ED, because it requires the energy spectrum for just two particles. When  $N$  is the number of unitcells, the cost is  $\sim N^3$ . This is in contrast to the cost of ED, which scales exponentially in  $N$ . Secondly, given that the projected Coulomb interaction does depend on the band characteristics, the comparison of the effective Haldane pseudopotential with those of the  $n$ LL can provide a useful alternative metric for the  $n$ LL-ness of Chern bands.

**5. Phase Diagram.** Within ED, we draw the many-body phase diagram over the parameter space of  $\theta \in [1.5^\circ, 3.0^\circ]$  and  $\epsilon_r \in [2, 10]$ , while holding other model parameters in Eq.(1) invariant. Over this parameter

space, we have confirmed that the system is fully valley polarized, and thus we perform ED on a single valley for  $N = 4 \times 6$  unitcells. Our primary focus is to identify the non-Abelian FQAH, whose lowest energy levels are in one-to-one correspondence with those in 1LL [21]. The resulting phase diagram is in [Fig.4(a)], which is compared with the value of  $S$  Eq.(2). We observe that the second moiré band-projected interaction remains close to the 1LL-projected Coulomb interaction for a wide range of angles and interaction strengths, with an optimal value in the vicinity of  $\theta \sim 2.2^\circ$  and  $\epsilon_r \sim 6$  [Fig.4(b)]. Globally, we find that the FQAH state is stabilized when the overall interaction strength is large enough, and when the projected interaction is 1LL-like, i.e.,  $S$  is small enough, revealing the efficacy of our metric Eq.(2).

**6. Conclusions.** We have shown that the behavior of the second moiré band in tMoTe<sub>2</sub> around  $\theta \sim 2.1^\circ$  exhibits remarkable parallels with 1LL. This similarity is not just limited to the band's characteristics, which fulfill the 1LL trace condition  $K = \int_{\text{BZ}} d^2\mathbf{k} \text{tr} \eta(\mathbf{k}) \approx 3$ , but also extends to the nature of the projected Coulomb interaction, which closely resembles the Haldane pseudopotentials in 1LL. These observations collectively hint at the possible emergence of a non-Abelian FQAH at  $\nu_h = 2 + 1/2$ , which we have confirmed through ED calculations. Moreover, we introduced a novel metric Eq.(2) of 1LL-ness of a band, which measures the similarity between the projected Coulomb interaction and the Haldane pseudopotentials in 1LL. This new metric  $S$  agrees reasonably well with the region where the FQAH is stabilized [Fig.4], when the interaction is strong enough.

When comparing our theoretical findings with experimental observations [11], we encounter several notable discrepancies. Firstly, the experiment does not seem to exhibit the valley-polarized FQAH that our model predicts at  $\nu_h = 2 + 1/2$ . Even more, our ED calculations, assuming the Coulomb interactions, predict a valley-polarized IQAH at  $\nu_h = 3$  [13], which is absent in the experiment [11]. These two together suggest that the actual interactions in tMoTe<sub>2</sub> at  $\theta \sim 2.1^\circ$  diverge from the simplest SU(2) valley-symmetric Coulomb interaction and are likely subject to significant renormalization. Such renormalization could undermine the FQAH at  $\nu_h = 2 + 1/2$ , while enhance the FQSH at  $\nu_h = 3$ .

Despite of this discrepancy with the currently-available experimental results [11], we note that there are various tuning parameters like displacement field, interlayer distance via pressure, and substrate variations for 2D twisted materials, which may lead to more favorable interactions for non-Abelian FQAHs than [11]. When combined with our theoretical finding, this makes the second moiré band of tMoTe<sub>2</sub> or twisted WSe<sub>2</sub> [36] a promising path for the 1LL-like non-Abelian FQAHs.

- *Note Added:* Near the completion of this work, we became aware of the two similar works [21, 37]. An



updated version (v2) of [21] identified a non-Abelian FQAH in the second moiré band of a skyrmion Chern band model, which is adiabatically-connected to the continuum model of twisted bilayer  $\text{MoTe}_2$  at  $\theta \sim 2.5^\circ$ , while [37] identified a non-Abelian FQAH in the second moiré band of the continuum model over a wide range of twist angles, using the parameters fitted to their DFT calculations of twisted bilayer  $\text{MoTe}_2$  at  $\theta \sim 1.9^\circ$ .

We thank Yong Baek Kim and Kwon Park for helpful discussions and Young-Woo Son for collaborations in related works. C.-E. A., W. L. and G.Y.C. are supported by Samsung Science and Technology Foundation under Project Number SSTF-BA2002-05, the NRF of Korea (Grant No.RS-2023-00208291, No.2023M3K5A1094810, No.2023M3K5A1094813) funded by the Korean Government (MSIT), the Air Force Office of Scientific Research under Award No.FA2386-22-1-4061, and Institute of Basic Science under project code IBS-R014-D1. K. Y. was supported by a KIAS individual grant (CG092501). A part of computations were supported by Center for Advanced Computation of KIAS. Y. K. is supported by NRF of Korea (2020R1C1C1006914, 2022M3H3A1098408) funded by the Korean Government (MSIT).

---

\* These authors contributed equally.

† gilyoungcho@postech.ac.kr

- [1] Y. Cao, V. Fatemi, A. Demir, S. Fang, S. L. Tomarken, J. Y. Luo, J. D. Sanchez-Yamagishi, K. Watanabe, T. Taniguchi, E. Kaxiras, *et al.*, *Nature* **556**, 80 (2018).
- [2] E. C. Regan, D. Wang, C. Jin, M. I. Bakti Utama, B. Gao, X. Wei, S. Zhao, W. Zhao, Z. Zhang, K. Yumigeta, *et al.*, *Nature* **579**, 359 (2020).
- [3] Y. Cao, D. Chowdhury, D. Rodan-Legrain, O. Rubies-Bigorda, K. Watanabe, T. Taniguchi, T. Senthil, and P. Jarillo-Herrero, *Physical review letters* **124**, 076801 (2020).
- [4] Y. Cao, V. Fatemi, S. Fang, K. Watanabe, T. Taniguchi, E. Kaxiras, and P. Jarillo-Herrero, *Nature* **556**, 43 (2018).
- [5] G. Chen, A. L. Sharpe, P. Gallagher, I. T. Rosen, E. J. Fox, L. Jiang, B. Lyu, H. Li, K. Watanabe, T. Taniguchi, *et al.*, *Nature* **572**, 215 (2019).
- [6] J. Cai, E. Anderson, C. Wang, X. Zhang, X. Liu, W. Holtzmann, Y. Zhang, F. Fan, T. Taniguchi, K. Watanabe, *et al.*, *Nature* **622**, 63 (2023).
- [7] Y. Zeng, Z. Xia, K. Kang, J. Zhu, P. Knüppel, C. Vaswani, K. Watanabe, T. Taniguchi, K. F. Mak, and J. Shan, *Nature* **622**, 69 (2023).
- [8] H. Park, J. Cai, E. Anderson, Y. Zhang, J. Zhu, X. Liu, C. Wang, W. Holtzmann, C. Hu, Z. Liu, *et al.*, *Nature* **622**, 74 (2023).
- [9] F. Xu, Z. Sun, T. Jia, C. Liu, C. Xu, C. Li, Y. Gu, K. Watanabe, T. Taniguchi, B. Tong, *et al.*, *Physical Review X* **13**, 031037 (2023).
- [10] Z. Lu, T. Han, Y. Yao, A. P. Reddy, J. Yang, J. Seo, K. Watanabe, T. Taniguchi, L. Fu, and L. Ju, *Nature* **626**, 759 (2024).
- [11] K. Kang, B. Shen, Y. Qiu, K. Watanabe, T. Taniguchi, J. Shan, and K. F. Mak, arXiv preprint arXiv:2402.03294 (2024).
- [12] X.-W. Zhang, C. Wang, X. Liu, Y. Fan, T. Cao, and D. Xiao, arXiv preprint arXiv:2311.12776 (2023).
- [13] See supplementary note for details.
- [14] T. Devakul, V. Crépel, Y. Zhang, and L. Fu, *Nature communications* **12**, 6730 (2021).
- [15] J. Dong, J. Wang, P. J. Ledwith, A. Vishwanath, and D. E. Parker, *Physical Review Letters* **131**, 136502 (2023).
- [16] N. Morales-Durán, N. Wei, J. Shi, and A. H. MacDonald, *Physical Review Letters* **132**, 096602 (2024).
- [17] J. Yu, J. Herzog-Arbeitman, M. Wang, O. Vafek, B. Bernevig, and N. Regnault, arXiv preprint arXiv:2309.14429 (2023).
- [18] Y. Jia, J. Yu, J. Liu, J. Herzog-Arbeitman, Z. Qi, N. Regnault, H. Weng, B. A. Bernevig, and Q. Wu, arXiv preprint arXiv:2311.04958 (2023).
- [19] A. P. Reddy, F. Alsallom, Y. Zhang, T. Devakul, and L. Fu, *Physical Review B* **108**, 085117 (2023).
- [20] M. Fujimoto, D. E. Parker, J. Dong, E. Khalaf, A. Vishwanath, and P. Ledwith, arXiv preprint arXiv:2403.00856 (2024).
- [21] A. P. Reddy, N. Paul, A. Abouelkomsan, and L. Fu, arXiv preprint arXiv:2403.00059 (2024).
- [22] N. Read and D. Green, *Physical Review B* **61**, 10267 (2000).
- [23] M. Oshikawa, Y. B. Kim, K. Shtengel, C. Nayak, and S. Tewari, *Annals of Physics* **322**, 1477 (2007).
- [24] L. Zhang and X.-Y. Song, arXiv preprint arXiv:2403.11478 (2024).
- [25] F. Wu, T. Lovorn, E. Tutuc, I. Martin, and A. MacDonald, *Physical review letters* **122**, 086402 (2019).
- [26] C. Xu, J. Li, Y. Xu, Z. Bi, and Y. Zhang, *Proceedings of the National Academy of Sciences* **121**, e2316749121 (2024).
- [27] C. Wang, X.-W. Zhang, X. Liu, Y. He, X. Xu, Y. Ran, T. Cao, and D. Xiao, *Physical Review Letters* **132**, 036501 (2024).
- [28] T. Wang, M. Wang, W. Kim, S. G. Louie, L. Fu, and M. P. Zaletel, arXiv preprint arXiv:2312.12531 (2023).
- [29] H. Li, U. Kumar, K. Sun, and S.-Z. Lin, *Physical Review Research* **3**, L032070 (2021).
- [30] A. P. Reddy and L. Fu, *Physical Review B* **108**, 245159 (2023).
- [31] S. Parameswaran, R. Roy, and S. L. Sondhi, *Physical Review B* **85**, 241308 (2012).
- [32] S. A. Parameswaran, R. Roy, and S. L. Sondhi, *Comptes Rendus Physique* **14**, 816 (2013).
- [33] P. J. Ledwith, A. Vishwanath, and D. E. Parker, *Physical Review B* **108**, 205144 (2023).
- [34] P. Potasz, N. Morales-Durán, N. C. Hu, and A. H. MacDonald, *Physical Review B* **109**, 045144 (2024).
- [35] A. M. Läuchli, Z. Liu, E. J. Bergholtz, and R. Moessner, *Physical Review Letters* **111**, 126802 (2013).
- [36] K. Kang, Y. Qiu, K. Watanabe, T. Taniguchi, J. Shan, and K. F. Mak, arXiv preprint arXiv:2402.04196 (2024).
- [37] C. Xu, N. Mao, T. Zeng, and Y. Zhang, arXiv preprint arXiv:2403.17003 (2024).